



Examining land surface phenology in the tropical moist forest eco-zone of South America

Boyi Liang^{1,2} · Xiaoqiu Chen¹ · Weiguang Lang¹ · Guohua Liu¹ · Yadvinder Malhi² · Sami Rifai²

Received: 27 December 2019 / Revised: 29 June 2020 / Accepted: 26 July 2020 / Published online: 1 August 2020
© ISB 2020

Abstract

Using leaf area index (LAI) data from 1981 to 2014 in the tropical moist forest eco-zone of South America, we extracted start (SOS) and end (EOS) dates of the active growing season in forest and savanna at each pixel. Then, we detected spatiotemporal characteristics of SOS and EOS in the two vegetation types. Moreover, we analyzed relationships between interannual variations of SOS/EOS and climatic factors, and simulated SOS/EOS time series based on preceding mean air temperature and accumulated rainfall. Results show that mean SOS and EOS ranged from 260 to 330 day of year (DOY) and from 150 to 260 DOY across the study region, respectively. From 1981 to 2014, SOS advancement is more extensive than SOS delay, while EOS advancement and delay are similarly extensive. For most pixels of forest and savanna in tropical moist forest eco-zone, preceding rainfall correlates predominantly negatively with SOS but positively with EOS, while the relationship between preceding temperature and phenophases is location-specific. In addition, preceding rainfall is more extensive than preceding temperature in simulating SOS, while both preceding rainfall and temperature play an important role for simulating EOS. This study highlights the reliability of using LAI data for long-term phenological analysis in the tropical moist forest eco-zone.

Keywords Tropical land surface phenology · Leaf area index · Linear trend · Statistical modeling · Rainfall and temperature

Introduction

Plant phenology is the study of the timing (and quantity) of annually recurring plant growth and reproductive phenomena, as well as the drivers of these events associated with endogenous and exogenous forces (Chen et al. 2017). Plant phenological variation is highly sensitive to climatic variation and has strong feedbacks on global carbon cycles and climate change (Piao et al. 2008; Richardson et al. 2013). Therefore, phenology has emerged recently as an important focus for ecological research (Piao et al. 2006).

Forests cover about 31% of the global land area (4000 M ha), in which 44% of the global forest area is

distributed in tropics (Keenan et al. 2015). As tropical forests constitute about 40% of the terrestrial phytomass (FAO 1993), a small variation in this biome may result in a significant change of the global carbon cycle (Phillips et al. 1998; Malhi et al. 2014; Brinck et al. 2017). Vegetation phenology is a key measure for assessing contribution of a biogeographical region to global climate change and carbon cycle. Numerous studies have focused on phenological detection in temperate and boreal vegetation but less attention has been paid to tropical vegetation phenology, especially at a long-term temporal scale and over a wide geographic area, which largely limits prediction capabilities of ecosystem production and carbon sequestration for the largest carbon pool. One of the reasons is the lack of long-term ground-observed phenological data in tropical areas. At the same time, the existing land surface phenological product (such as MCD12Q2) has large errors in tropics (Chapman et al. 2005; Zhang et al. 2012).

To date, both in situ observations and remotely sensed data have been used to examine phenological variation and its climatic controls for tropical vegetation (Zhang et al. 2003; Fisher et al. 2006; Richardson et al. 2009). The former is usually for detecting plant individual phenology at discrete

✉ Xiaoqiu Chen
cxq@pku.edu.cn

¹ College of Urban and Environmental Sciences, Laboratory for Earth Surface Processes of the Ministry of Education, Peking University, Beijing 100871, People's Republic of China

² Environmental Change Institute, School of Geography and the Environment, University of Oxford, South Parks Road, Oxford OX1 3QY, UK

sites (Wolfe et al. 2005; Cleland et al. 2007; Liang et al. 2012), while the latter is commonly for monitoring vegetation phenology at plant community and landscape scales (Lüdeke et al. 1996; Richardson et al. 2006).

Tropical moist forest eco-zone is mainly distributed in South America, Southern parts of Africa, South and East Asia, and North Australia, which contains different vegetation types, such as forest, savanna, shrubland, and cropland (FAO and SDSU 2009). Vegetation density in the tropical moist forest eco-zone is significantly higher than that of temperate regions, and phenological feature (seasonality) there is much more distinct than tropical rainforest. Therefore, vegetation phenology in the tropical moist forest eco-zone can be effectively detected by remotely sensed data (Verger et al. 2016). In addition, tropical moist forest region has more evident rainy and dry seasons through each year than tropical dry forest, and therefore, it is suitable for modeling the synergistic effect of rainfall and temperature on vegetation phenology. So far, most studies on vegetation phenology in tropical moist forest eco-zone were based on in situ phenological observation data for specific species during short periods of time (Kushwaha and Singh 2005; Saha et al. 2005; Williams et al. 2008; Bajpai et al. 2012; Bajpai et al. 2017; Rankine et al. 2017). Spatiotemporal patterns of vegetation phenology in the tropical moist forest eco-zone at large scale and their relation to climatic factors remain poorly understood. More effective satellite data and robust approaches should be employed to identify vegetation phenology and its climatic controls in this area.

In this study, we first extracted the start (SOS) and end (EOS) dates of the active growing season in forest and savanna of the tropical moist forest eco-zone in South America using leaf area index (LAI) data. Then, we analyzed spatiotemporal characteristics of SOS and EOS dates in the study areas. Finally, we created preceding mean temperature/accumulated rainfall-based phenology models for simulating interannual variation of SOS and EOS dates at pixel scales. The scientific questions we intend to address are as follows: (i) What are the spatiotemporal patterns of land surface vegetation phenology for forest and savanna in the tropical moist forest eco-zone? (ii) What are major climate drivers of interannual variations of land surface vegetation phenology for forest and savanna in this eco-zone? (iii) Are phenological models developed for temperate trees suitable for simulating interannual variation of land surface phenology of forest and savanna in this eco-zone?

Materials and methods

Study area

We selected tropical moist forest eco-zone from the global eco-zone (FAO and SDSU 2009) in middle and eastern South America as the study area (Fig. 1), which mainly covers

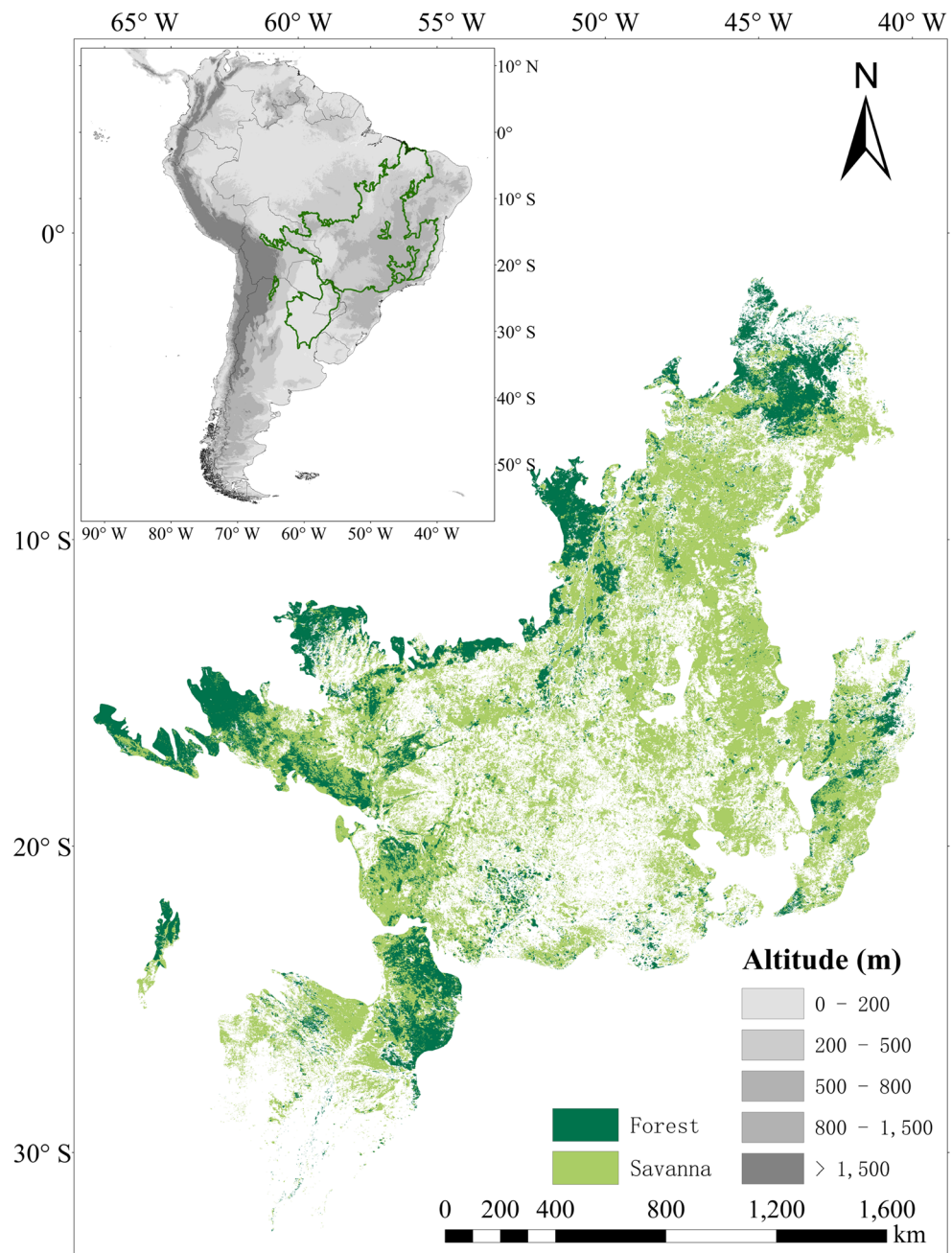
southeastern parts of Brazil and Paraguay, the middle part of Bolivia, and the northeastern part of Argentina, with altitude ranging from 500 to 1500 m. This region was defined based on seasonal precipitation and temperature regimes, and roughly contains the tropical monsoon climate and tropical savanna climate of the Köppen climate classification system (Beck et al. 2018). Vegetation growth cycles in this area are constrained by seasonal migrations of Intertropical Convergence Zone and Subtropical High that bring in alternating rainy and dry seasons. In general, annual average temperature is above 18 °C and dry season lasts about 3–5 months in each year (FAO 2012). The annual maximum temperature is about 27 °C and occurs normally in February, while the annual minimum temperature is about 24 °C and appears commonly in July. The annual range of temperatures is less than 6 °C. By contrast, rainfall is characterized by alternating dry and rainy seasons. The dry season ranges usually from April to September. The smallest monthly rainfall appears in August (less than 10 mm) and the largest monthly rainfall occurs in December (about 300 mm). Our study focuses on tropical moist forest and savanna because they are main natural vegetation types in tropical moist forest eco-zone and account for 11.3% and 35.6% of the total area, respectively. Ranges of the two vegetation types were determined according to the International Geosphere-Biosphere Program (IGBP) Global Land Cover Characterization (GLCC) data with a spatial resolution of 1 km (Loveland et al. 2000).

Remotely sensed data and phenophase extraction

The Global Land Surface Satellite (GLASS) LAI data from 1981 to 2014 were acquired from Chinese National Earth System Science Data Sharing Infrastructure website (<http://www.geodata.cn/thematicView/GLASS.html>) (Liang et al. 2013; Xiao et al. 2014). The values of LAI were estimated from AVHRR (before 2000) and MODIS (after 2000) surface-reflectance time series data using general regression neural networks (Zhao et al. 2013). The spatial resolution is 5 km and temporal interval is 8 days. In the production process of GLASS LAI, the time series cloud detection (TSCD) algorithm was employed. This algorithm searches the clear-sky reference first, and then discriminates pixels with and without clouds by detecting a sudden change of reflectance (Tang et al. 2013). This process reduced the influence of clouds to reflectance to the maximum extent, especially in tropics.

Here, we used Savitzky-Golay filter (Savitzky and Golay 1964) to remove outliers of data sources and relative threshold method to identify the start and end dates of the active growing season (defined as the period when leaves are most plentiful within a year). Two symmetrical thresholds were used to identify the two phenophases. Specifically, EOS was determined as the date when LAI fell to the value of 80% from the range between maximum LAI and minimum LAI, while SOS was identified as the date when LAI rose to the value of

Fig. 1 Location of the tropical moist forest eco-zone in South America and distribution of forest and savanna



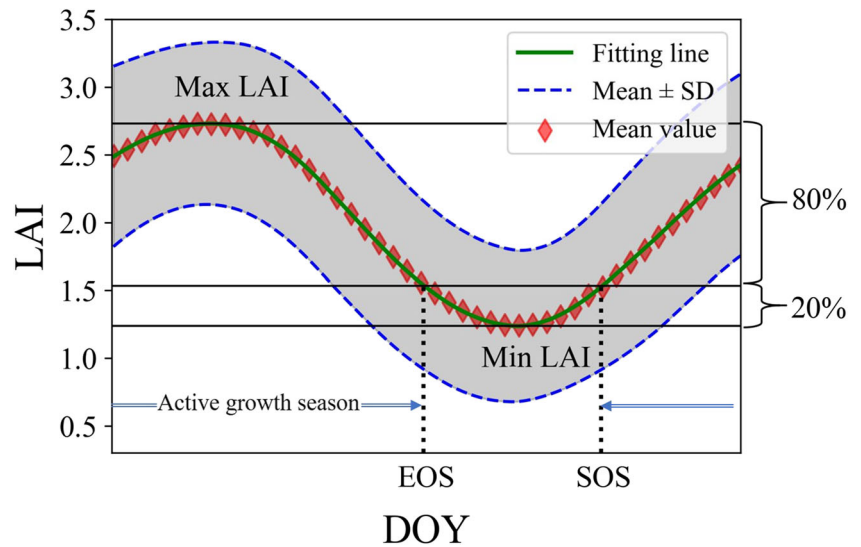
20% from the range between minimum LAI and maximum LAI (Fig. 2). Meanwhile, we used Fourier analysis (Schwarzenberg-Czerny 1989; Bloomfield 2004) to identify the vegetation areas with single growth cycle to ensure the reliability of SOS and EOS extraction.

Meteorological data

The European Union Water and Global Change project (<http://www.eu-watch.org>) provides a gridded European Union Water and Global Change-Forcing-Data-ERA-Interim data

product (Weedon et al. 2014; Ren et al. 2018). It contains eight meteorological variables from 1979 to 2014 with a spatial resolution of 0.5°. In this study, we used daily rainfall and daily mean air temperature data from 1981 to 2014 to analyze climatic effects on interannual variation of SOS and EOS by resampling remotely sensed LAI from 5 km into spatial resolution of 0.5° using bicubic method. For unifying spatial resolution of vegetation type (1 km), LAI (0.5°), and meteorological data (0.5°), we overlaid LAI and meteorological data on vegetation type map and extracted LAI and meteorological data values for each pixel of the vegetation types.

Fig. 2 Schematic diagram for determining start and end dates of the active growing season. The red dots represent reconstructed mean LAI data after processing. The green solid line is the fitted curve. The blue-dashed lines show mean LAI ± standard deviation. The black dots indicate SOS and EOS dates and their corresponding relative thresholds



Mann-Kendall trend test

We used the Mann-Kendall (MK) test to calculate trends of SOS/EOS over the 34 years at each pixel. Compared with simple linear regression, the MK test does not ask for specific distribution of original data, and the slope is insensitive to outliers (Yue et al. 2002).

To determine whether a linear trend exists in a time series ($X = x_1, x_2, x_3, \dots, x_n$), a statistic is constructed as follows:

$$S = \sum_{j=1}^{n-1} \sum_{k=j+1}^n \text{sign}(x_k - x_j) \quad 1 \leq j < k \leq n \quad (1)$$

$$\text{where } \text{sign}(x_k - x_j) = \begin{cases} 1 & \text{if } (x_k - x_j) > 0 \\ 0 & \text{if } (x_k - x_j) = 0 \\ -1 & \text{if } (x_k - x_j) < 0 \end{cases} \quad (2)$$

Under the assumption that the data are independent and identically distributed (iid), the mean and variance of the S statistic in Eq. (1) are given by Kendall and Gibbons (1990) as:

$$E(S) = 0 \quad (3)$$

$$\text{Var}(S) = \frac{1}{18} [n(n-1)(2n+5)] \quad (4)$$

By using the statistic S and variance $\text{Var}(S)$, a standardized test statistic Z is calculated as follows when n is larger than 10:

$$Z = \begin{cases} \frac{S-1}{\sqrt{\text{Var}(S)}} & \text{for } S > 0 \\ 0 & \text{for } S = 0 \\ \frac{S+1}{\sqrt{\text{Var}(S)}} & \text{for } S < 0 \end{cases} \quad (5)$$

The standardized M-K statistic Z has a normal distribution, u , with mean of 0 and variance of 1. At a given significance level, α , if $|Z| > u_{(1-\alpha/2)}$, the null hypothesis at α significance

level is rejected, which indicates that the time series X has a significant temporal trend. If $Z > 0$, there is an increasing trend, while if $Z < 0$, there is a decreasing trend. The slope is defined as:

$$\beta = \text{Median} \left(\frac{x_k - x_j}{k - j} \right) \quad 1 \leq j < k \leq n \quad (6)$$

Phenology model and its evaluation

As temporal variations of tropical plant phenology are triggered not only by air temperature but also by rainfall, we used mean air temperature and accumulated rainfall during the optimum length period to simulate SOS and EOS dates by creating regression models. The basic hypothesis is that the year-to-year variation of a phenological event occurrence date at a station is mainly influenced by year-to-year variation of climatic factors within a particular length period (LP) during and before its occurrence at the same station (Chen and Xu 2012). The LP in this study is determined as the time period at a pixel, during which the interannual variation in mean temperature or accumulated rainfall affects the interannual variation of SOS/EOS most remarkably. The computation process was carried out by following steps. First, we defined the number of days between the earliest and latest dates (day of year, DOY) of a specific SOS or EOS timing series at a given pixel from 1981 to 2014 as the basic length period (bLP). Then, we calculated backwards (to earlier time direction) the mean air temperature and accumulated rainfall time series at the pixel during bLP + mLP. Here, mLP was a moving length period prior to the earliest date of SOS or EOS timing series, which moved with a step length of 1 day. The maximum mLP was set to 60 days for SOS and 30 days for EOS because mean temperature and accumulated rainfall prior to these periods were usually assumed to have less effects on interannual variation of SOS or EOS date. The LP is defined as follows [Eq. (7)]:

$$LP = bLP + mLP \quad (7)$$

Furthermore, we correlated SOS and EOS dates with mean temperature and accumulated rainfall during different LP at each pixel from 1981 to 2014, respectively, and obtained the optimum LP with the largest partial correlation coefficients (absolute value) corresponding to temperature and rainfall at each pixel, respectively. The significance levels of partial correlation were evaluated based on two-tailed significance tests. Finally, we created unitary (taking either mean temperature or accumulated rainfall during the optimum length period as the independent variable, Eqs. (8) and (9)) and binary (taking both mean temperature and accumulated rainfall during the optimum length periods as independent variables, Eq. (10)) regression equations to fit SOS/EOS (dependent variable) at each pixel. The unitary and binary regression equations are shown as follows:

$$\text{Phenophase} = a + b \times T_{\text{optimum}} \quad (8)$$

$$\text{Phenophase} = a + b \times P_{\text{optimum}} \quad (9)$$

$$\text{Phenophase} = a + b_1 \times T_{\text{optimum}} + b_2 \times P_{\text{optimum}} \quad (10)$$

where Phenophase denotes phenological occurrence date (SOS/EOS); P_{optimum} is the accumulated rainfall during the optimum length period, and T_{optimum} is the mean temperature during the optimum length period; a is the intercept; b , b_1 , and b_2 are the slopes.

For comparing fitting accuracy of SOS and EOS among the three types of regression equations at each pixel, the root mean square error (RMSE) and the small-sample corrected Akaike information criterion (AICc) were used. RMSE (Eq. (11)) measures the mean error of fitted SOS and EOS dates, while AICc (Eq. (12)) rates models in terms of parsimony and efficiency.

$$\text{RMSE} = \sqrt{\frac{\sum_{i=1}^n (\text{obs}_i - \text{fit}_i)^2}{n}} \quad (11)$$

$$\text{AICc} = n \times \ln \left(\frac{\sum_{i=1}^n (\text{obs}_i - \text{fit}_i)^2}{n} \right) + \frac{2n(k+1)}{n-k-2} \quad (12)$$

where obs_i and fit_i are the observed and fitted SOS/EOS dates in year i , respectively; n is the number of years; k is the number of parameters.

Results

Spatial patterns of mean date and linear trend of SOS and EOS

The multi-year mean SOS ranges from 260 to 330 DOY (accounting for more than 99% of all pixels) with a spatial

tendency from southwest (earlier SOS) to northeast (later SOS). Specifically, pixels with SOS earlier than 270 DOY (late September) are concentrated in the southwestern region but pixels with SOS later than 310 DOY (early November) are located in the northeastern region. The multi-year mean EOS ranges from 150 (late May) to 260 DOY (mid September) (accounting for more than 98% of all pixels) with a spatial tendency from south (earlier EOS) to northeast (later EOS) (Fig. 3a, b).

For different vegetation types, forest shows earlier SOS (with an average date of 285 DOY) than savanna (with an average date of 289 DOY) but later EOS (with the average date of 196 DOY) than savanna (with the average date of 183 DOY) (Fig. 4). Thus, forest has the longer mean growing season than savanna in the study region. Compared with forest, the spatial standard deviation of multi-year mean EOS in savanna is much smaller, which indicates that spatial differentiation of EOS in savanna is obviously smaller than that in forest (Fig. 4).

With respect to linear trends of SOS and EOS from 1981 to 2014, SOS shows a significant advancement ($p < 0.05$) in 19.1% of pixels and a significant delay ($p < 0.05$) in 10.8% of pixels. The pixels with a significant advancement are distributed mostly in middle parts of the study region, while the pixels with a significant delay are located mainly in northeastern and southwestern parts of the region. For EOS, significant advancement and delay ($p < 0.05$) were detected in 14.2% and 13.0% of pixels, respectively, in which significant advancement appeared mainly in south and northeast parts, while significant delay occurred predominantly in west and east parts (Fig. 5).

Percentages of pixels with advanced and delayed trends in SOS and EOS vary with forest and savanna. For SOS, a significantly advanced trend ($p < 0.05$) appeared at 10.7% of pixels for forest and 16.3% of pixels for savanna, while a significantly delayed trend ($p < 0.05$) occurred at 14.1% of pixels for forest and 11.6% of pixels for savanna. For EOS, the percentage of pixels with significant delay ($p < 0.05$) accounts for 16.2% in forest and 14.6% in savanna. By contrast, the percentage of pixels with significant advancement ($p < 0.05$) takes up 12.1% and 13.8% of pixels for forest and savanna, respectively (Fig. 6).

Relationship between interannual variations of SOS/EOS and climatic factors

The main climate driver for both SOS and EOS in forest and savanna is preceding rainfall instead of temperature. Negative correlations between SOS and preceding rainfall account for 92.9% and 93.6% of forest and savanna pixels, respectively, and significantly ($p < 0.05$) negative correlations were found at 56.9% (forest) and 56.8% (savanna) of pixels. That is, more preceding rainfall may induce earlier SOS. On the contrary,

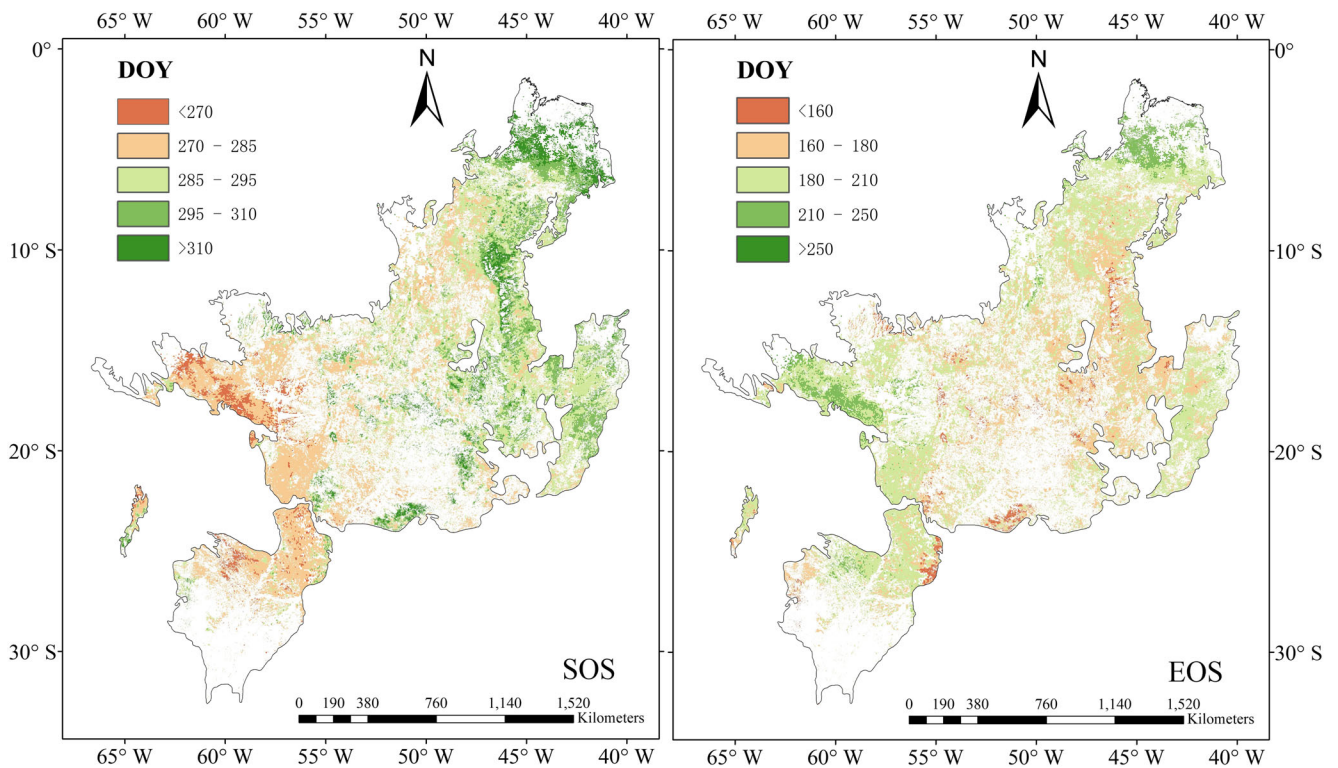
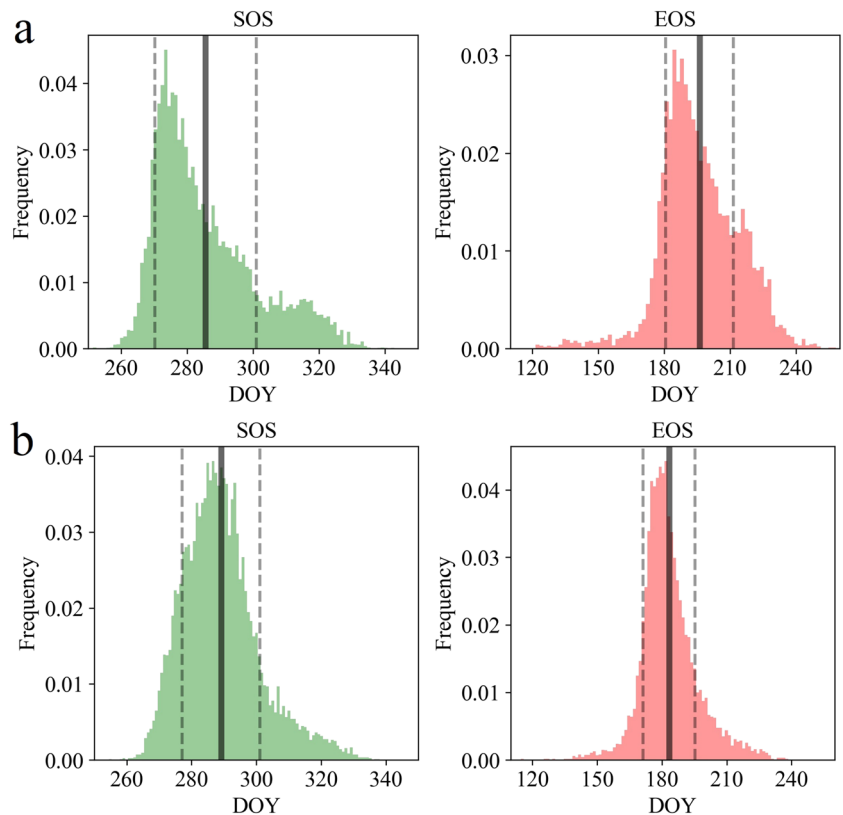


Fig. 3 Spatial distribution of multi-year mean SOS and EOS from 1981 to 2014 in tropical moist forest and savanna

pixels with positive correlations between EOS and rainfall account for 59.1% and 66.8% in forest and savanna,

respectively, and significantly ($p < 0.05$) positive correlations were detected at 23.8% (forest) and 32.2% (savanna) of pixels.

Fig. 4 Frequency of multi-year mean SOS and EOS for forest (a) and savanna (b). Vertical solid line denotes the regional mean value; vertical-dashed lines denote the regional mean value \pm spatial standard deviation



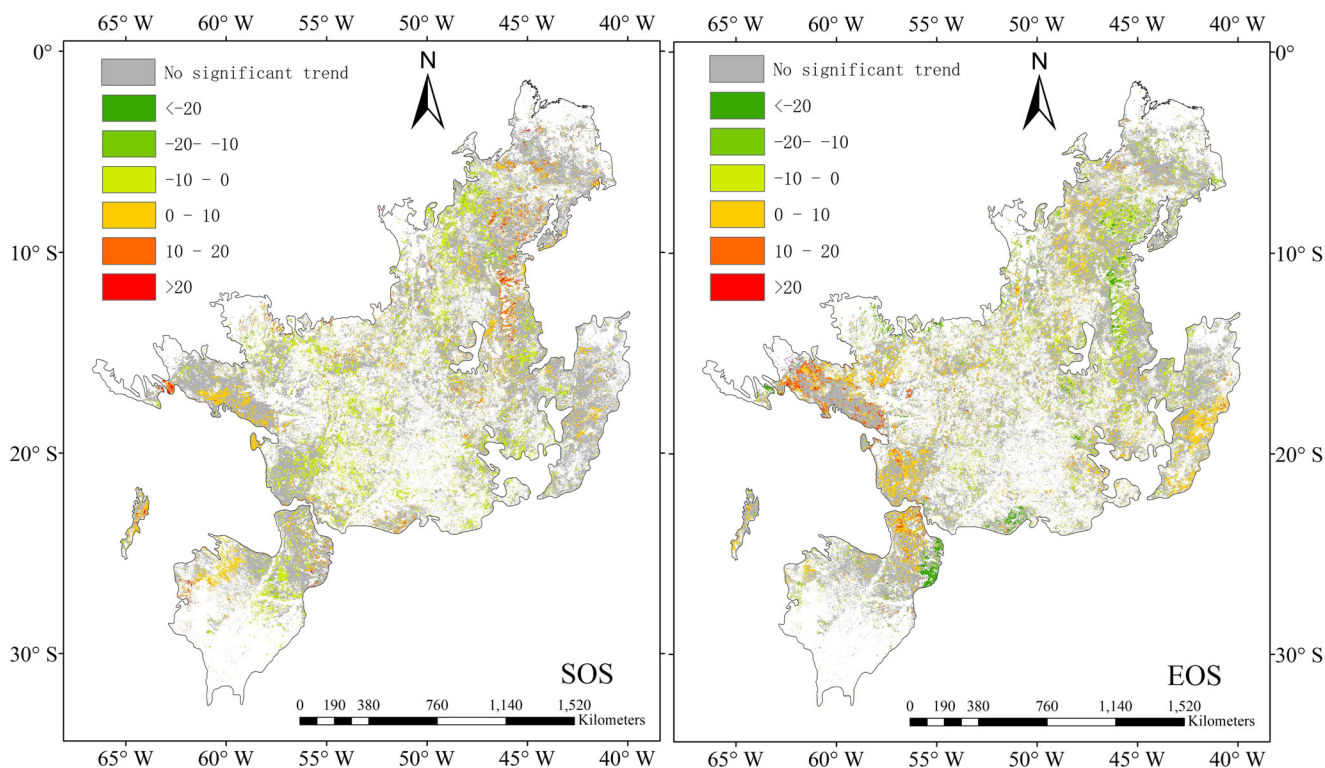


Fig. 5 Spatial distribution of linear trends (in days per decade) of SOS and EOS

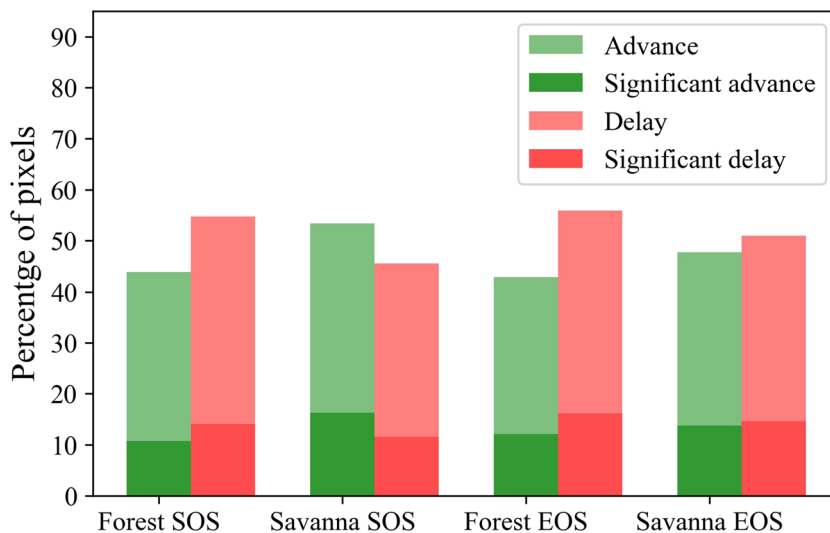
Namely, more preceding rainfall may delay EOS. This shows that the effect of rainfall on SOS (mostly negative impact) is more extensive than on EOS (mostly positive impact) for the two vegetation types. In comparison, no predominant correlation directions between SOS/EOS and preceding mean temperature for the two vegetation types were detected, and correlation significance levels between SOS/EOS and preceding mean temperature are much lower than those between SOS/EOS and preceding rainfall. Specifically, SOS correlates significantly ($p < 0.05$) negatively with preceding temperature at 4.1% (forest) and 4.3% (savanna) of pixels but significantly

($p < 0.05$) positively with preceding temperature at 16.2% (forest) and 19.5% (savanna) of pixels. Similarly, EOS correlates significantly ($p < 0.05$) negatively with preceding temperature at 17.6% (forest) and 24.5% (savanna) of pixels but significantly ($p < 0.05$) positively with preceding temperature at 7.9% (forest) and 6.0% (savanna) of pixels.

SOS and EOS modeling

We constructed three kinds of regression models for simulating SOS and EOS time series at each pixel in forest and

Fig. 6 Percentage of pixels with advanced and delayed trends of SOS and EOS for forest and savanna



savanna, and then selected the pixel-specific optimum models by means of the smallest AICc values. The results show that optimum SOS models created by rainfall alone account for 46.5% of forest pixels and 48.9% of savanna pixels, whereas optimum SOS models created by temperature alone and combination of rainfall and temperature take up 26.5% and 26.6% of forest pixels, and 23.4% and 28.2% of savanna pixels, respectively (Fig. 7). However, EOS was best fitted by temperature-based models at 47.1% (forest) and 35.5% (savanna) of pixels, and by rainfall-based models at 39.0% (forest) and 46.1% (savanna) of pixels. In addition, rainfall- and temperature-combining models fitted EOS best only at 13.8% (forest) and 18.5% (savanna) of pixels (Fig. 7). Thus, it can be seen that preceding rainfall is more extensive and important than preceding temperature and combination of rainfall and temperature in simulating SOS in forest and savanna, while preceding temperature and rainfall separately play an important role for simulating EOS in forest and savanna.

It is worth pointing out that optimum SOS models created by combination of rainfall and temperature have the smallest average RMSE (10.2 days for forest and 8.5 days for savanna), while optimum SOS models created by temperature alone have the largest average RMSE (16.8 days in forest and 15.2 days for savanna). In terms of EOS, optimum models created by combination of rainfall and temperature also have the smallest RMSE (13.6 days for forest and 9.1 days for savanna). However, average RMSE of optimum models created by rainfall alone (19.8 days) are larger than those of models created by temperature alone (16.7 days) for forest, while average RMSE of optimum models created by temperature alone (11.4 days) are larger than those of models created by rainfall alone (10.1 days) for savanna (Fig. 8). Further analyses show that for forest, pixels with a RMSE less than 10 days accounts for 23.3%/32.7% of rainfall-based SOS/EOS models, 0.07%/50% of temperature-based SOS/EOS

models, and 53.5%/62.5% of rainfall-temperature combination SOS/EOS models, respectively. For savanna, however, pixels with a RMSE less than 10 days account for 23.4%/75.3% of rainfall-based SOS/EOS models, 0.27%/65% of temperature-based SOS/EOS models, and 73.6%/78.3% of rainfall-temperature combination SOS/EOS models, respectively. Overall, models considering integrative effect of rainfall and temperature can significantly improve fitting accuracy of SOS and EOS of both forest and savanna, and fitting accuracy of savanna SOS and EOS based on the three types of models is higher than that of forest SOS and EOS (Fig. 8).

Discussion

In this study, long-term and large-scale phenological features of forest and savanna in the tropical moist forest eco-zone of South America were examined using GLASS LAI. We selected the tropical moist forest eco-zone released by FAO as the study area because GLASS LAI data were tested under the framework of this eco-zone classification. It should be noted that this eco-climatic region contains several vegetation types, such as forest, shrubland, savanna, grassland, permanent wetland, and cropland/natural vegetation mosaic, among which forest and savanna account for nearly 50% of total areas. Thus, our study focused on the two major vegetation types. To reveal the vegetation growing season of forest and savanna and its climate drivers, we analyzed and modeled SOS and EOS changes.

In previous studies, different relative thresholds (from 10 to 50%) were selected to determine SOS and EOS, in which the 20% relative threshold was mostly used (Yu et al. 2010; Cong et al. 2012). Verger et al. (2016) used 30% and 40% threshold to detect SOS and EOS of global vegetation based on the GEOCLIM-LAI product, while Prasad et al. (2007) applied 35% threshold to determine SOS and EOS in tropical forest of

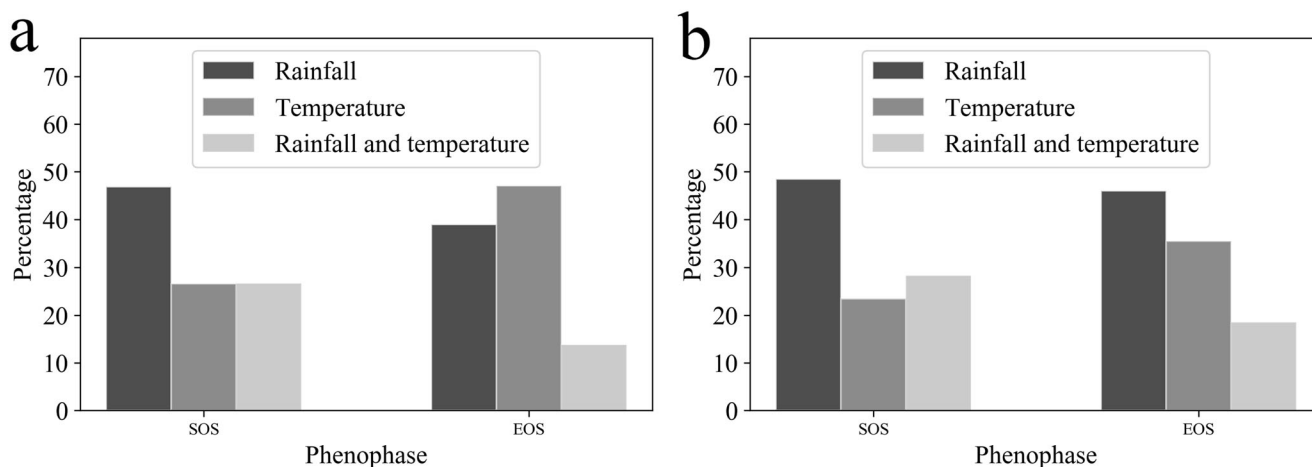


Fig. 7 Percentage of pixels of the optimum models created by rainfall, temperature, and combination of rainfall and temperature for forest (a) and savanna (b)

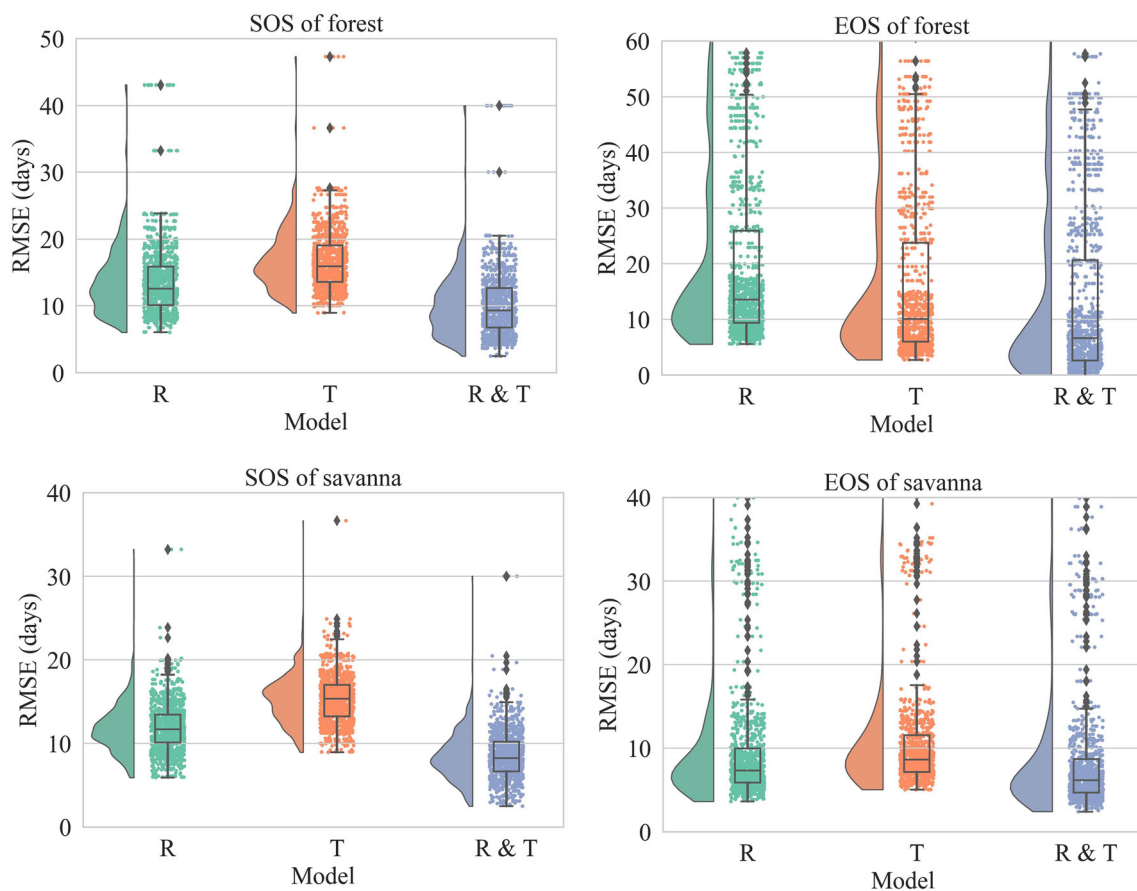


Fig. 8 Box plot of the distribution in RMSE of SOS and EOS models created by rainfall (R), temperature (T), and combination of rainfall and temperature (R&T) for different vegetation types. The solid line in the

middle of a box is the mean value. The upper and lower edges of a box denote 25th and 75th percentile of RMSE from all pixels. The upper and lower whiskers denote the range of RMSE from all pixels

India. Thus, there are no universal standards for selecting thresholds for different vegetation types. In addition, unlike temperate vegetation, tropical forests have no distinct dormancy period during 1 year. As tropical vegetation growth is characterized by replacement of old leaves by new ones (Myneni et al. 1997; Zhang 2015), different vegetation types have diverse seasonal growth regimes. In this study, we employed 20% threshold for extracting SOS and EOS, mainly considering the specific characteristics of vegetation growth in the research region. As a distinct dormancy period cannot be detected on LAI curves in the tropical moist forest eco-zone of South America, we redefined the growing season as the period of most vigorous vegetation growth within a year, namely, the active growing season.

From the result of multi-year mean SOS and EOS for forest and savanna (Fig. 4), we can see that forest tends to have earlier SOS, later EOS and longer active growth season than savanna. The potential explanation is the relatively longer rainy season in forest than in savanna. Moreover, spatial difference of EOS in forest is obviously larger than that in savanna (Fig. 4), which might be caused by larger spatial heterogeneity of regimes of preceding rainfall in forest areas than

savanna areas, because EOS of both forest and savanna is mainly triggered by preceding rainfall. As forest is discretely distributed at the edge of the study area but savanna is concentrated in the middle and eastern parts (Fig. 1), spatial difference in regimes of preceding rainfall in forest might be larger than those in savanna. Consequently, larger EOS spatial difference in forest than in savanna could be expected. During the past decades, a spring phenology advancement and an autumn phenology delay, as well as a growing season lengthening, have been detected using remotely sensed and ground-observed phenology data across most temperate regions of the Northern Hemisphere (Zhou et al. 2001; Menzel et al. 2006; Schwartz et al. 2006; Chen and Xu 2012), which was attributed mainly to climate warming and would directly affect the carbon cycle and ecosystem productivity (Keeling et al. 1996; Richardson et al. 2010; Keenan et al. 2014). However, long time series phenological trend analyses in tropical areas are scarce. Our study in the tropical moist forest eco-zone indicates that the percentages of pixels with significant advanced SOS and with significant delayed EOS in the tropical moist forest eco-zone are generally less than those in temperate regions. This might be due to the fact that SOS and EOS in the

study region are influenced not only by preceding temperature but also by preceding rainfall. Further correlation analyses show that preceding rainfall plays even a more important role than preceding temperature in triggering SOS and EOS.

Regarding relationships between SOS/EOS and climatic factors, preceding rainfall correlates negatively with SOS but positively with EOS for both forest and savanna. That is, more preceding rainfall can result in an advanced SOS but a delayed EOS, which is consistent with a phenological study in tropical areas (Zhang et al. 2005). The key function of rainfall on leaf phenology was also demonstrated by other studies. For instance, preceding rainfall has stronger relationship with SOS than EOS in a tropical deciduous forest of Mexico, because expansion of leaves is greatly influenced by water availability, while leaf abscission depends on multiple environmental factors (Bullock and Solis-Magallanes 1990). In north Australian tropical savanna, leaf flushing and leaf fall dates have good temporal coherency with rainy season (Williams et al. 1997), and rainfall variability is a major environmental cue of vegetation phenology variability in the North Australian Tropical Transect (Ma et al. 2013). In addition, Bobée et al. (2012) revealed that the first rain event has high synchronization with vegetation SOS in Sahelian environments, while lack of rainfall at the beginning of rainy season may delay vegetation emergence phase. It should be noted that the total rainfall during the dry season (from July to September) took up only 4.3% of annual accumulated rainfall in our study region. Thus, plants lived in a state of extreme water scarcity prior to SOS. However, monthly mean air temperatures during July–September had already achieved 23.5–24.0 °C that was high enough for triggering SOS. This shows that rainfall but not temperature is the restriction factor of SOS in the study region. By contrast, EOS was indirectly triggered by preceding rainfall amount, because soil and plant could store water from rainy season (Borchert 1980, 1998; De Bie et al. 1998). That is, although the rainy season had almost been terminated, the stored water during the rainy season still affected the time of EOS.

It is well known that higher preceding temperature induces mostly earlier SOS and later EOS dates in temperate regions (Cleland et al. 2007; Piao et al. 2015; Chen et al. 2017). However, at most pixels of forest and savanna in the tropical moist forest eco-zone of South America, preceding mean temperature is positively correlated with SOS but negatively correlated with EOS. This might be associated with high temperature-induced evaporation increase and water restriction. Namely, intensive evaporation may cause seasonal water shortage in soil and organs of vegetation, and induce later SOS and earlier EOS.

Conclusions

In this study, we analyzed spatial patterns of mean date and linear trend of SOS and EOS in forest and savanna of the

tropical moist forest eco-zone of South America. Moreover, we detected the relationship between SOS/EOS and climatic factors and constructed three types of models to simulate SOS and EOS time series. The conclusions are as follows:

1. Mean SOS and EOS ranged from 260 to 330 DOY and from 150 to 260 DOY in the study region, respectively. Forest has earlier SOS, later EOS, and longer active growth season than savanna. From 1981 to 2014, SOS advancement is more extensive than SOS delay, while EOS advancement and delay are similarly extensive.
2. Preceding rainfall is the decisive factor in triggering SOS and EOS for both forest and savanna. The effect of rainfall on SOS (mostly negative impact) is more extensive than on EOS (mostly positive impact).
3. Preceding rainfall plays a more extensive and important role than preceding temperature and combination of rainfall and temperature for simulating SOS in forest and savanna, while preceding rainfall and temperature separately play an important role for simulating EOS in forest and savanna.

Funding information This research was funded by the National Natural Science Foundation of China under grant nos. 41771049 and 41471033, and the scholarship of the China Scholarship Council.

References

- Bajpai O, Kumar A, Mishra AK, Sahu N (2012) Phenological study of two dominant tree species in tropical moist deciduous forest from the northern India. *Int J Bot* 8(2):66–72
- Bajpai O, Pandey J, Chaudhary L (2017) Periodicity of different phenophases in selected trees from Himalayan Terai of India. *Agrofor Syst* 91(2):363–374
- Beck HE, Zimmermann NE, McVicar TR, Vergopolan N, Berg A, Wood EF (2018) Present and future Köppen-Geiger climate classification maps at 1-km resolution. *Sci Data* 5:180214
- Bloomfield P (2004) *Fourier analysis of time series: an introduction*. John Wiley and Sons, Hoboken
- Bobée C, Ottlé C, Maignan F, De Noblet-Ducoudré N, Manguis P, Lézine A-M, Ndiaye M (2012) Analysis of vegetation seasonality in Sahelian environments using MODIS LAI, in association with land cover and rainfall. *J Arid Environ* 84:38–50
- Borchert R (1980) Phenology and ecophysiology of tropical trees: *Erythrina poeppigiana* OF cook. *Ecology* 61(5):1065–1074
- Borchert R (1998) Responses of tropical trees to rainfall seasonality and its long-term changes. In: *Potential Impacts of Climate Change on Tropical Forest Ecosystems*. Springer, Dordrecht, pp 241–253
- Brinck K, Fischer R, Groeneveld J, Lehmann S, De Paula MD, Pütz S, Sexton JO, Song D, Huth A (2017) High resolution analysis of tropical forest fragmentation and its impact on the global carbon cycle. *Nat Commun* 8:14855
- Bullock SH, Solis-Magallanes JA (1990) Phenology of canopy trees of a tropical deciduous forest in Mexico. *Biotropica* 22:22–35
- Chapman CA, Chapman LJ, Struhsaker TT, Zanne AE, Clark CJ, Poulsen JR (2005) A long-term evaluation of fruiting phenology: importance of climate change. *J Trop Ecol* 21(1):31–45

- Chen X, Xu L (2012) Phenological responses of *Ulmus pumila* (Siberian Elm) to climate change in the temperate zone of China. *Int J Biometeorol* 56(4):695–706
- Chen X, Zhang W, Ren S, Lang W, Liang B, Liu G (2017) Temporal coherence of phenological and climatic rhythmicity in Beijing. *Int J Biometeorol* 61(10):1733–1748
- Cleland EE, Chuine I, Menzel A, Mooney HA, Schwartz MD (2007) Shifting plant phenology in response to global change. *Trends Ecol Evol* 22(7):357–365
- Cong N, Piao S, Chen A, Wang X, Lin X, Chen S, Han S, Zhou G, Zhang X (2012) Spring vegetation green-up date in China inferred from SPOT NDVI data: a multiple model analysis. *Agric For Meteorol* 165:104–113
- De Bie S, Ketner P, Paasse M, Geerling C (1998) Woody plant phenology in the West Africa savanna. *J Biogeogr* 25(5):883–900
- FAO (1993) Forest Resources Assessment 1990: Tropical Countries. FAO Forestry Paper 112
- FAO (2012) Global ecological zones for FAO forest reporting: 2010 update. Forest Resources Assessment Working Paper 179. Food and Agriculture Organization of the United Nations, Rome
- FAO J, SDSU U (2009) The 2010 global forest resources assessment remote sensing survey: an outline of the objectives, data, methods and approach. Forest Resources Assessment Working Paper 155
- Fisher JJ, Mustard JF, Vadeboncoeur MA (2006) Green leaf phenology at Landsat resolution: scaling from the field to the satellite. *Remote Sens Environ* 100(2):265–279
- Keeling CD, Chin J, Whorf T (1996) Increased activity of northern vegetation inferred from atmospheric CO₂ measurements. *Nature* 382(6587):146–149
- Keenan TF, Gray J, Friedl MA, Toomey M, Bohrer G, Hollinger DY, Munger JW, O’Keefe J, Schmid HP, Wing IS, Yang B, Richardson AD (2014) Net carbon uptake has increased through warming-induced changes in temperate forest phenology. *Nat Clim Chang* 4(7):598–604
- Keenan RJ, Reams GA, Achard F, de Freitas JV, Grainger A, Lindquist E (2015) Dynamics of global forest area: results from the FAO global forest resources assessment 2015. *For Ecol Manag* 352:9–20
- Kendall MG, Gibbons JD (1990) Rank correlation methods. Edward Arnold, London
- Kushwaha C, Singh K (2005) Diversity of leaf phenology in a tropical deciduous forest in India. *J Trop Ecol* 21(1):47–56
- Liang L, Schwartz MD, Fei S (2012) Photographic assessment of temperate forest understorey phenology in relation to springtime meteorological drivers. *Int J Biometeorol* 56(2):343–355
- Liang S, Zhang X, Xiao Z, Cheng J, Liu Q, Zhao X (2013) Global Land Surface Satellite (GLASS) products: algorithms, validation and analysis. Springer Science and Business Media, Berlin
- Loveland T, Reed B, Brown J, Ohlen D, Zhu Z, Yang L, Merchant J (2000) Development of a global land cover characteristics database and IGBP DISCover from 1 km AVHRR data. *Int J Remote Sens* 21(6–7):1303–1330
- Lüdeke MK, Ramage PH, Kohlmaier G (1996) The use of satellite NDVI data for the validation of global vegetation phenology models: application to the Frankfurt Biosphere Model. *Ecol Model* 91(1–3):255–270
- Ma X, Huete A, Yu Q, Coupe NR, Davies K, Broich M, Ratana P, Beringer J, Hutley LB, Cleverly J (2013) Spatial patterns and temporal dynamics in savanna vegetation phenology across the North Australian Tropical Transect. *Remote Sens Environ* 139:97–115
- Malhi Y, Farfán Amézquita F, Doughty CE, Silva-Espejo JE, Girardin CA, Metcalfe DB, Aragão LE, Huaraca-Quispe LP, Alzamora-Taype I, Eguiluz-Mora L (2014) The productivity, metabolism and carbon cycle of two lowland tropical forest plots in south-western Amazonia, Peru. *Plant Ecol Divers* 7(1–2):85–105
- Menzel A, Sparks TH, Estrella N, Koch E, Aasa A, Ahas R, Alm-Kübler K, Bissolli P, Og B, Briede A (2006) European phenological response to climate change matches the warming pattern. *Global change biology* 12(10):1969–1976
- Myneni RB, Keeling C, Tucker CJ, Asrar G, Nemani RR (1997) Increased plant growth in the northern high latitudes from 1981 to 1991. *Nature* 386(6626):698
- Phillips OL, Malhi Y, Higuchi N, Laurance WF, Núñez PV, Vásquez RM, Laurance SG, Ferreira LV, Stern M, Brown S (1998) Changes in the carbon balance of tropical forests: evidence from long-term plots. *Science* 282(5388):439–442
- Piao S, Fang J, Zhou L, Ciais P, Zhu B (2006) Variations in satellite-derived phenology in China’s temperate vegetation. *Glob Chang Biol* 12(4):672–685
- Piao S, Ciais P, Friedlingstein P, Peylin P, Reichstein M, Luyssaert S, Margolis H, Fang J, Barr A, Chen A (2008) Net carbon dioxide losses of northern ecosystems in response to autumn warming. *Nature* 451(7174):49–52
- Piao S, Yin G, Tan J, Cheng L, Huang M, Li Y, Liu R, Mao J, Myneni RB, Peng S (2015) Detection and attribution of vegetation greening trend in China over the last 30 years. *Glob Chang Biol* 21(4):1601–1609
- Prasad VK, Badarinath K, Eaturu A (2007) Spatial patterns of vegetation phenology metrics and related climatic controls of eight contrasting forest types in India—analysis from remote sensing datasets. *Theor Appl Climatol* 89(1–2):95–107
- Rankine C, Sánchez-Azofeifa G, Guzmán JA, Espirito-Santo M, Sharp I (2017) Comparing MODIS and near-surface vegetation indexes for monitoring tropical dry forest phenology along a successional gradient using optical phenology towers. *Environ Res Lett* 12(10):105007
- Ren S, Chen X, Lang W, Schwartz MD (2018) Climatic controls of the spatial patterns of vegetation phenology in mid-latitude grasslands of the Northern Hemisphere. *J Geophys Res Biogeosci* 123(8):2323–2336
- Richardson AD, Bailey AS, Denny EG, MARTIN CW, O’KEEFE J (2006) Phenology of a northern hardwood forest canopy. *Glob Chang Biol* 12(7):1174–1188
- Richardson AD, Braswell BH, Hollinger DY, Jenkins JP, Ollinger SV (2009) Near-surface remote sensing of spatial and temporal variation in canopy phenology. *Ecol Appl* 19(6):1417–1428
- Richardson AD, Black TA, Ciais P, Delbart N, Friedl MA, Gobron N, Hollinger DY, Kutsch WL, Longdoz B, Luyssaert S, Migliavacca M, Montagnani L, Munger JW, Moors E, Piao S, Rebmann C, Reichstein M, Saigusa N, Tomelleri E, Vargas R, Varlagin A (2010) Influence of spring and autumn phenological transitions on forest ecosystem productivity. *Philos Trans R Soc Lond Ser B Biol Sci* 365(1555):3227–3246
- Richardson AD, Keenan TF, Migliavacca M, Ryu Y, Sonnentag O, Toomey M (2013) Climate change, phenology, and phenological control of vegetation feedbacks to the climate system. *Agric For Meteorol* 169:156–173
- Saha S, BassiriRad H, Joseph G (2005) Phenology and water relations of tree sprouts and seedlings in a tropical deciduous forest of South India. *Trees* 19(3):322–325
- Savitzky A, Golay MJ (1964) Smoothing and differentiation of data by simplified least squares procedures. *Anal Chem* 36(8):1627–1639
- Schwartz MD, Ahas R, Aasa A (2006) Onset of spring starting earlier across the Northern Hemisphere. *Glob Chang Biol* 12(2):343–351
- Schwarzenberg-Czerny A (1989) On the advantage of using analysis of variance for period search. *Mon Not R Astron Soc* 241(2):153–165
- Tang H, Yu K, Geng X, Zhao Y, Jiang K, Liang S (2013) A time series method for cloud detection applied to MODIS surface reflectance images. *Int J Digit Earth* 6:157–171
- Verger A, Filella I, Baret F, Peñuelas J (2016) Vegetation baseline phenology from kilometeric global LAI satellite products. *Remote Sens Environ* 178:1–14
- Weedon GP, Balsamo G, Bellouin N, Gomes S, Best MJ, Viterbo P (2014) The WFDEI meteorological forcing data set: WATCH

- Forcing Data methodology applied to ERA-Interim reanalysis data. *Water Resour Res* 50(9):7505–7514
- Williams R, Myers B, Muller W, Duff G, Eamus D (1997) Leaf phenology of woody species in a north Australian tropical savanna. *Ecology* 78(8):2542–2558
- Williams LJ, Bunyavejchewin S, Baker PJ (2008) Deciduousness in a seasonal tropical forest in western Thailand: interannual and intra-specific variation in timing, duration and environmental cues. *Oecologia* 155(3):571–582
- Wolfe DW, Schwartz MD, Lakso AN, Otsuki Y, Pool RM, Shaulis NJ (2005) Climate change and shifts in spring phenology of three horticultural woody perennials in northeastern USA. *Int J Biometeorol* 49(5):303–309
- Xiao Z, Liang S, Wang J, Chen P, Yin X, Zhang L, Song J (2014) Use of general regression neural networks for generating the GLASS leaf area index product from time-series MODIS surface reflectance. *IEEE Trans Geosci Remote Sens* 52(1):209–223
- Yu H, Luedeling E, Xu J (2010) Winter and spring warming result in delayed spring phenology on the Tibetan Plateau. *Proc Natl Acad Sci* 107(51):22151–22156
- Yue S, Pilon P, Cavadas G (2002) Power of the Mann–Kendall and Spearman's rho tests for detecting monotonic trends in hydrological series. *J Hydrol* 259(1–4):254–271
- Zhang X (2015) Reconstruction of a complete global time series of daily vegetation index trajectory from long-term AVHRR data. *Remote Sens Environ* 156:457–472
- Zhang X, Friedl MA, Schaaf CB, Strahler AH, Hodges JC, Gao F, Reed BC, Huete A (2003) Monitoring vegetation phenology using MODIS. *Remote Sens Environ* 84(3):471–475
- Zhang XY, Friedl MA, Schaaf CB, Strahler AH, Liu Z (2005) Monitoring the response of vegetation phenology to precipitation in Africa by coupling MODIS and TRMM instruments. *J Geophys Res Atmos* 110:(D12103)
- Zhang XY, Friedl MA, Tan B, Goldberg MD, Yu Y (2012). Long-term detection of global vegetation phenology from satellite instruments. In: *Phenology and climate change*. InTech, London, pp 297–320
- Zhao X, Liang S, Liu S, Yuan W, Xiao Z, Liu Q, Cheng J, Zhang X, Tang H, Zhang X (2013) The Global Land Surface Satellite (GLASS) remote sensing data processing system and products. *Remote Sens* 5(5):2436–2450
- Zhou L, Tucker CJ, Kaufmann RK, Slayback D, Shabanov NV, Myneni RB (2001) Variations in northern vegetation activity inferred from satellite data of vegetation index during 1981 to 1999. *J Geophys Res Atmos* 106(D17):20069–20083

Publisher's note Springer Nature remains neutral with regard to jurisdictional claims in published maps and institutional affiliations.